ARTICLE

INNOVATION AND EMERGING TECHNOLOGIES

# Design and fabrication of a three-dimensional asymmetric neonate lung model to study surfactant transport in airways

Hannah Combs [1], Jacob Heiss [1], Lillian Beaty [1], Joseph Gavriloff [1] & Hossein Tavana [1,*]

**Neonatal respiratory distress syndrome is a potentially life-threatening condition that is often treated with the delivery of exogenous surfactants through a process called surfactant replacement therapy. This therapy includes the administration of the liquid surfactant through an endotracheal tube and mechanical ventilation. Due to the difficulty of imaging neonate lungs during this therapy, the success of surfactant delivery is often determined by observational techniques and evaluation of blood oxygen levels. The limitation of imaging creates challenges in evaluating the distribution of surfactant in airways. To address this limitation, we designed a computational, eight-generation, asymmetric neonate lung model using morphometric data to mimic the geometric structure of the human airway tree and fabricated it using an additive manufacturing technique. We used our model to study two-aliquot delivery of a clinically rated liquid surfactant under two different orientations to evaluate its distribution in airways. Our study offers a complex lung airway tree design that mimics the native geometry of the human airway tree to enable studies of therapeutics transport in airways.**

***Keywords*: Neonatal Respiratory Distress Syndrome; Asymmetric Airway Tree; Lung Airway Model; Distribution Index; Plug Stalling.**

## INTRODUCTION

The lungs contain a series of airways that is divided by dichotomous branching and become more numerous as they penetrate deeper into the chest cavity[1]. The lung airway tree begins at the trachea, which is known as the generation zero ($z = 0$) airway, where the conducting zone begins[2]. The conducting zone is where air is transported in and out of the lungs and spans from generation zero to the terminal bronchioles. As bronchiole tubes branch off from their preceding airway into a new generation, they decrease in diameter and length. The airway tree transitions from the conducting zone to the respiratory zone that includes respiratory bronchioles and terminates at alveolar sacs[2,3]. The alveolar sacs are sites of gas exchange to oxygenate the blood and remove carbon dioxide. Presence of pulmonary surfactant in the liquid lining of alveoli is critical to this process. Pulmonary surfactant is synthesized and secreted by Type II alveolar epithelial cells, adsorbs at the air–liquid interface of alveoli, and reduces surface tension to facilitate normal breathing[4,5]. The lack of or insufficient surfactant results in a high surface tension, possibly collapsing the alveoli and impeding proper gas exchange[6–9].

In preterm infants born approximately prior to 24 weeks of gestation, the lungs are underdeveloped and severely lack natural surfactant[10,11], increasing the likelihood of lung collapse or even death[12]. To treat the neonatal respiratory distress syndrome (NRDS), exogenous surfactant is delivered to the neonate through an endotracheal tube in a process known as neonatal surfactant replacement therapy (NSRT)[13]. The instilled surfactant forms a plug in the trachea, which is then propagated through the lung airway tree using mechanical ventilation[14,15]. The goal is to deliver surfactant to the gas exchange units to reduce the air–liquid surface tension and prevent them from collapsing[15]. The success of NSRT depends on homogeneous surfactant distribution through the lung airway tree. Multiple variables including the position of the infant during treatment and the number of aliquots determine surfactant distribution in airways[16–20]. The current methods for evaluating the success of this therapy are mainly observational such as monitoring oxygen levels or observing the chest movements of the infant during respiration[11]. Although there have been advancements in early detection of NRDS using techniques such as lung ultrasound (LUS), there are still significant limitations such as inability to image through barriers of air due to reflection and lack of standardized diagnostic protocols[21,22]. NRDS remains one of the leading causes of mortality in preterm infants[12]. The lack of safe imaging techniques hampers quantitative evaluation and optimization of surfactant delivery in neonates.

To address this limitation, computational studies have been conducted to study surfactant transport through neonatal lung airways. Several such studies have used simple geometries such as single bifurcating airway models to investigate effects of orientation of airways in the gravitational field, types and properties of surfactant solutions, and fluid properties on splitting of surfactant plugs at bifurcations and deposition of airway walls[1,23]. A more complex computational airway

[1]Department of Biomedical Engineering, The University of Akron, Akron, OH 44325, USA. *Correspondence should be addressed to: H.T. (tavana@uakron.edu).

Received 6 May 2024; accepted 2 July 2024; published online 31 August 2024; doi:10.1142/S2737599424500063

model was also developed to simulate liquid surfactant instillation in a symmetric lung airway tree of a 1-kg neonate and to evaluate the efficiency and homogeneity of the distribution[19]. Another computational study simulated surfactant transport through an asymmetric model of a rat airway tree and showed an inhomogeneous distribution compared to that in a symmetric airway tree[24]. Several benchtop models have also been developed for empirical studies. Some of these include macroscale and microscale single bifurcating units that contain only a parent tube and its two daughter tubes[25-27], a three-generation, planar model made with PDMS[28], and a more complex eight-generation, 3D, symmetric model developed using additive manufacturing[29]. Over two decades ago, an ex vivo model was also used to investigate transport of instilled surfactant in airways. A surfactant containing a radiopaque tracer was instilled in an excised rat lung in a vertical orientation and X-ray imaging was used to capture surfactant transport during multiple breath cycles and help quantify its distribution throughout the lung[30]. Despite being a physiological model, rat lungs have a significantly different geometry from human lungs and cannot reliably predict intratracheal therapeutics delivery in humans.

Despite the progress made to study surfactant transport in models of neonatal airways, there is still a need for a physical model that mimics the geometry of airway tree to help evaluate distribution of liquid surfactant instillation under clinically relevant conditions such as changes in the orientation of neonate and multiple aliquots delivery[27,31]. Here, we designed and fabricated an asymmetric airway tree using morphologically relevant dimensions of human lungs. We quantified liquid surfactant distribution among the five lobes of the airway tree and evaluated how the asymmetry of airways and the orientation of the model in gravitational field affect surfactant distribution in the conducting zone. We found that airways in gravitationally favored lobes received a greater volume of the instilled surfactant. Furthermore, we found that the asymmetry of the model hindered transport of surfactant boli in airways compared to that in a previously established symmetric model[31]. Our bioengineered model mimics distinct characteristic of the native lungs and offers a tool to study and optimize liquid surfactant delivery in neonates.

## METHODS

### Working fluid

Infasurf, a natural calfactant with a phospholipid concentration of 35 mg/mL, was generously provided by ONY Inc. and used. The properties of Infasurf include a surface tension of $\gamma = 25$ dynes cm$^{-1}$ and a density of $\rho = 0.980$ g cm$^{-3}$.[5,29,31]

### Experimental setup and liquid plug generation

The asymmetric neonate lung model was designed and fabricated using SOLIDWORKS and additive manufacturing techniques, respectively[27,29,31]. A custom-designed bracket was secured to a Plexiglass platform for increased stability of the model. Subsequently, the model was mounted to the custom bracket to ensure accuracy of adjusting the orientation of airways during experiments. The Plexiglass platform was positioned and secured on a Panavise[27]. An accelerometer was attached to the Plexiglass platform, allowing for accurate changes to orientation characterized with a roll angle ($\alpha$). The change in roll angle simulated lateral rolling of the preterm infant from a supine position ($\alpha = 0°$) to a lateral decubitus position, where they are fully rotated onto right side ($\alpha = 90°$) or left side ($\alpha = -90°$) of the body.

Experiments were conducted with the model positioned at $\alpha = 0°$, $\alpha = 90°$, and $\alpha = -90°$. First, each model was exposed to high-frequency oxygen plasma for 10 minutes to render the internal surface of the airways hydrophilic[15,31]. Next, the internal surface of the airways was pre-wet by placing a 250 µL plug of distilled water inside the tracheal tube and propagating it through the airways. The distilled water was lightly aspirated out of all terminal airways to ensure that the bronchial pathway was coated with a layer of water and to verify that airways were clear of obstructions or clogs. A thin film of water remained throughout the airways to create a pre-wet environment on the wall of the airways.

Two aliquots of Infasurf surfactant were instilled and propagated through the airway model at different time points. For the first aliquot, a 140 µL plug of surfactant was instilled in the tracheal tube using a positive displacement pipette. Silicon tubing (Tygon) was used to attach the trachea of the lung model to a 100 mL syringe (Norm-Ject). The syringe was secured to a syringe pump (Chemyx Inc., Stafford, TX). Forced air was infused from the pump to propagate the surfactant plug throughout the airways of the lung model. The residual plugs from the aliquot were lightly aspirated to eliminate obstructions within the terminal airways, while maintaining a thin surfactant film on airway walls. A second 140 µL aliquot was instilled and propagated through the airway model as described previously.

### Imaging, image analysis, and statistical analysis

Videos of surfactant transport were recorded from four views at 30 fps. The four views were recorded using a Nikon D3100 with a macro lens (Tamron 272ENII, 90 mm), Canon VIXIA HF S100 with a 58 mm ultraviolet lens (SUNPAK), an iPad (Model A1701), and a cell phone (Google Pixel 6). All videos were imported to ImageJ (NIH) and trimmed to the same number of frames. To quantify the plug volume in each airway, the length of each surfactant plug ($P_l$), the distance from the beginning of the airway to the top of the plug ($X_1$), and the distance from the end of the airway to the bottom of the plug ($X_2$) were measured[31]. To verify the accuracy of the measurements, the sum of the three values was calculated to ensure matching the known length of the airway. Following verification of the measurements, the plug length and airway diameter were used to calculate the volume of the plug inside each airway. The plug volume was used to calculate a distribution index (DI), which was defined as the volume of surfactant solution that enters each of the five lobes of the airways to the instilled volume. The plug volume was also used to develop heat maps that displayed the distribution of the surfactant solution through five generations of the lung model. Four replicates of all experiments were completed to assess effects of orientation and a preexisting film on the distribution of surfactant within the asymmetric neonate lung model.

### Quantifying a distribution index

The three lobes emerging at the $z = 2$ generation and the two lobes emerging at the $z = 3$ generation were labeled as the UR, $LR_p$, $LR_a$, the LL, and UL. The volume of the plugs in each airway was calculated as $V = (\pi/3)\, P_l\, ((r_1^2 + r_2^2) + (r_1 \times r_2))$, where $r_1$ and $r_2$ are the radii of the airway where the top and bottom of each plug are located, and $P_l$ is the length of the surfactant plug. Two different radii were used because of the tapering geometry of airway tubes. The volume of the plug in each lobe was quantified from the respective airway and used to calculate the DI as $DI = V_{z=2} / V_{=0}$ for the UR, LL, and UL lobes and $DI = V_{z=3} / V_{=0}$ for $LR_p$ and $LR_a$ lobes.

## RESULTS

### Design principles of asymmetric airway model

To construct the asymmetric lung airway model, we extracted morphologically relevant dimensions from an extensive dataset that was obtained by taking measurements of silica lung castings[32,33]. The castings were fabricated from the lungs of an adult male cadaver during an autopsy. The dataset comprehensively covered airway measurements from the trachea to the terminal bronchial tubes. Specifically, we captured data on the length of airways ($l$), the diameter of airways (d), and the angles of airway segment branching ($\theta$) for generations $z = 0$–$7$[32,33]. We scaled the length of the adult male airways to that of a neonate by $l_N = l_A \times (d_N / d_A)$, where $l_N$ is the length of the neonate airway, $l_A$ is the length of the measured adult airway, $d_N$ is the diameter of the trachea for a neonate, and

$d_A$ is the diameter of the adult trachea. We first constructed the tracheal tube with a diameter of 3.5 mm and length of 20.9 mm[29,31]. Diameters of the daughter airways were determined by utilizing diameter ratios of 0.87 and 0.67 with respect to the parent airway and assigned to the major and minor airways, respectively[33–35]. The daughter airway with the larger diameter was labeled as the major airway, while the one with the smaller diameter was labeled as the minor airway (**Fig. 1a**)[33]. This differentiation enabled us to properly assign the angles of airway segment branching to the major and minor daughter airways. The angle of the airway segment branching, also known as the bifurcation angle (θ), was constructed from the centerline of the parent airway for the major and minor airways (**Fig. 1a**). To ensure a seamless transition from each parent tube to the daughter tubes, all airways contained a 13.5% tapered diameter[29]. Following the third generation, all daughter airways rotated 90° from the centerline of their parent airway to mimic the anatomic rotation of airways inside the chest cavity[29,33].

Using the abovementioned protocol and calculated dimensions, we developed the model in SOLIDWORKS using features including lofted boss/base, lofted cut, and reference planes[29]. We first constructed the tracheal tube and then attached a sketch onto the bottom of the trachea that contained the proper dimensions for the bifurcation zone and daughter airways (**Fig. 1a**). Using the sketch as a guideline, we created the bifurcation zone (**Fig. 1b**) and then attached the daughter airways to the bifurcation zone, creating the $z = 0–1$ part of the model (**Fig. 1c**). Following this process, we constructed each airway individually and added it to the previous parent airway to fully construct all eight generations containing 255 airway tubes (**Fig. 1d**)[29].

## Fabrication of asymmetric airway model

We fabricated the model using an additive manufacturing technique known as stereolithography (SLA). SLA is a 3D printing technique that uses a laser to partially cure a photopolymer resin onto a build platform layer by layer to the specifications of the computational model[36]. Using a FormLabs 3B+ SLA resin printer, we fabricated the model with a transparent resin called Clear V4 (**Fig. 1e**). The resin allowed for a high, 25 µm resolution printing. Following the fabrication of the model, we conducted a series of rigorous post-processing steps to increase the clarity of the model and ensure that all airways were cleared of residual resin that could otherwise impact the surfactant transport process. We first placed the model in an agitated IPA bath (Form Wash) for 1 hour to remove residual resin. Next, we transferred the model into a reservoir containing Tripropylene glycol monomethyl ether (TPM) to soak for 24 hours. Then, we connected the model to a submersible pump (Domica Pump) using Tygon tubing and flushed it with IPA for 1 hour. Following these post-processing steps, we used a thin wire to verify that all airways were clear of residual resin plugs. We used a Dremel tool with a 0.3 mm diameter drill bit to gently clear any residues from terminal airways.

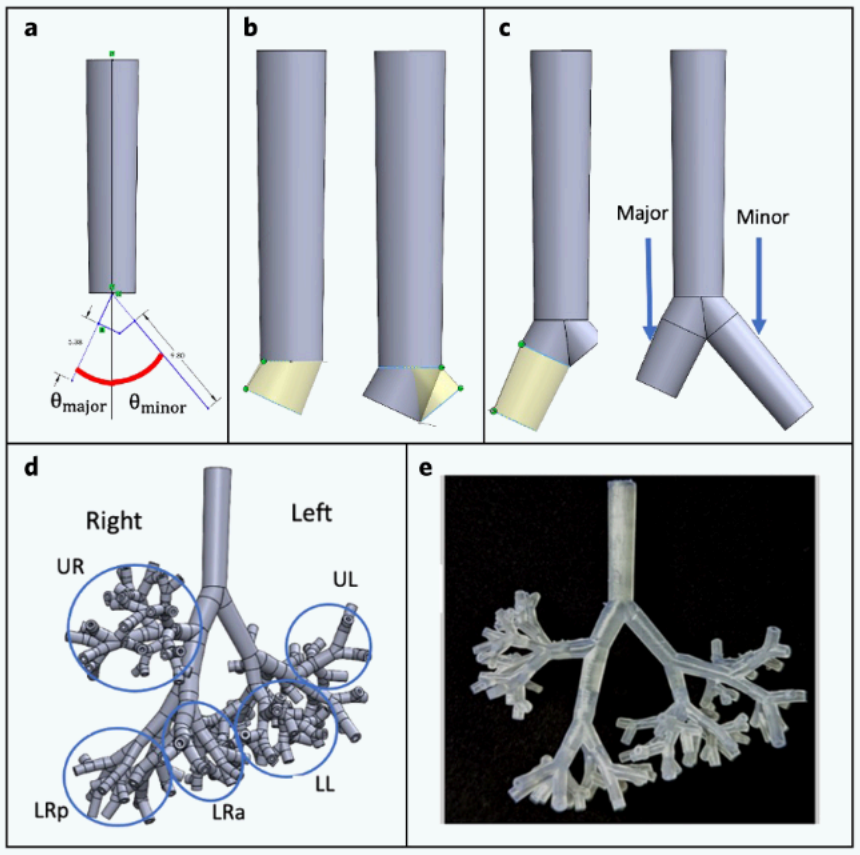


**Figure 1** (**a**) Construction of the trachea tube with the addition of a sketch that aids in the fabrication of the bifurcation zone and daughter tubes, (**b**) the fabrication of the bifurcation zone created at specified angle, (**c**) the fabrication of the daughter tubes, creating z = 0–1, (**d**) a computational model of the eight-generation airway tree with labeling for five lobes as the upper right (UR), lower right posterior ($LR_p$), lower right anterior ($LR_a$), lower left (LL), and upper left (UL), and (**e**) the corresponding fabrication model.

## Distribution of instilled surfactant

To determine the distribution of instilled surfactant in lung airways, we conducted surfactant delivery experiments and evaluated effects of an asymmetric geometry, lateral rotation of airway tree, and a preexisting surfactant film in the airways[31]. We positioned the model on the test platform (**Fig. 2**) at $\alpha = 0°$, $\alpha = 90°$, or $\alpha = -90°$, instilled a surfactant plug inside the tracheal tube, and propagated it using forced air at a flow rate of 100 mL/min, which corresponds to a capillary number (Ca) of 0.05[31]. The capillary number is defined as the relative effects of viscous and surface forces and is represented by $Ca = \mu u/\gamma$, where $\mu$ is dynamic viscosity, $u$ is velocity, and $\gamma$ is surface tension.

We quantified the total volume of surfactant where the lung airways divide into the five lobes (**Fig. 1d**). At $\alpha = 0°$ for the first aliquot, the instilled surfactant divided relatively evenly, resulting in $DI_{UR} = 0.13 \pm 0.001$, $DI_{LR_a} = 0.08 \pm 0.009$, $DI_{LR_p} = 0.09 \pm 0.008$, $DI_{LL}$ $0.08 \pm 0.008$, and $DI_{UL} = 0.14 \pm 0.003$ ($p < 0.05$; **Fig. 3a, b** and Movie S1). At $\alpha = 0°$ for the second aliquot, the surfactant plug did not divide as evenly as the first aliquot, giving $DI_{UR} = 0.12 \pm 0.001$, $DI_{LR_a} = 0.09 \pm 0.013$, $DI_{LR_p} = 0.08 \pm 0.011$, $DI_{LL} = 0.07 \pm 0.005$, and $DI_{UL} = 0.19 \pm 0.013$ ($p < 0.05$; **Fig. 3a, c** and Movie S2). As expected, the DI values did not add up to a value of one because of surfactant loss on the walls of the airways from the propagating plug prior to reaching this junction. The sum of the indices increased from the first aliquot to the second one, indicating reduced surfactant loss on the walls due to a preexisting surfactant film.

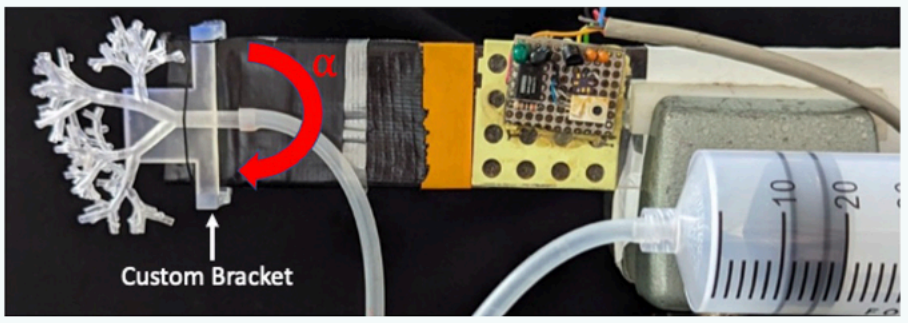


**Figure 2** Experimental setup of lung model attached to a custom bracket that is secured to a Plexiglass platform. The platform is secured to a Panavise which is used to modify the roll angle (α) quantified using an accelerometer. The model is attached to the syringe pump using Tygon tubing.

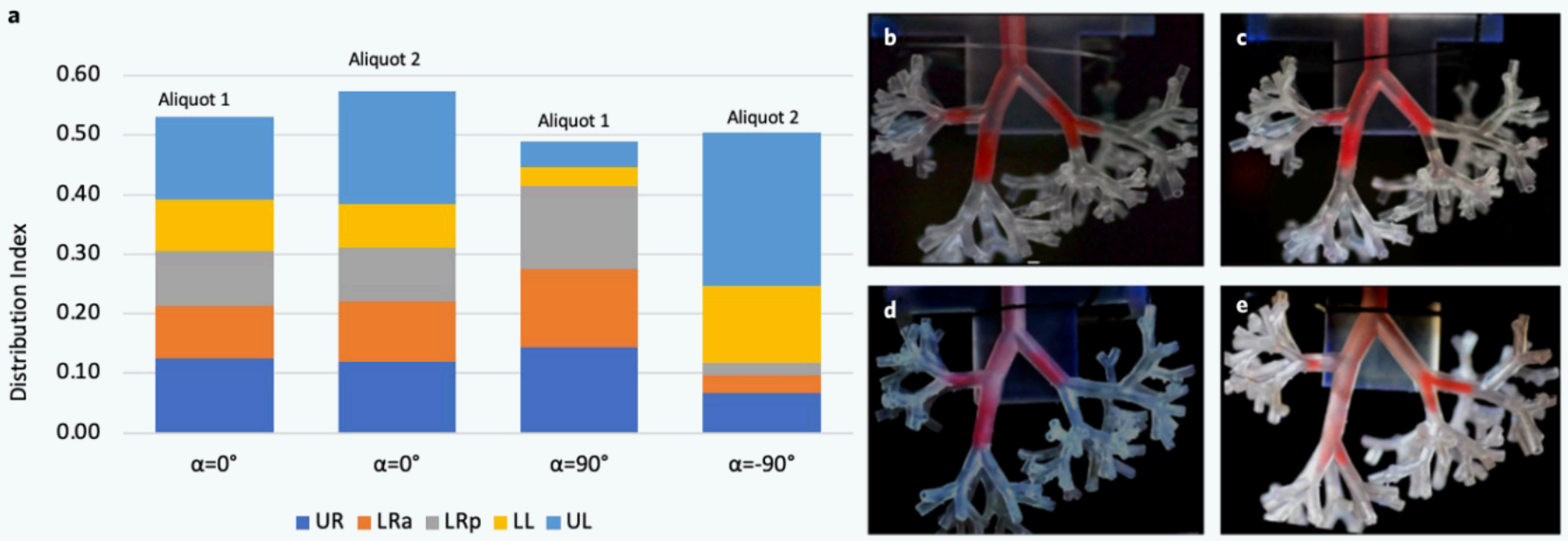


**Figure 3** (**a**) The distribution index for UR, LRp, LRa, LL, and UL lobes at $\alpha = 0°$, 90°, and –90° for aliquot 1 and aliquot 2. Surfactant distribution for (**b**) aliquot 1 at $\alpha = 0°$, (**c**) aliquot 2 at $\alpha = 0°$, (**d**) aliquot 1 at $\alpha = 90°$, and (**e**) aliquot 2 at $\alpha = -90°$.

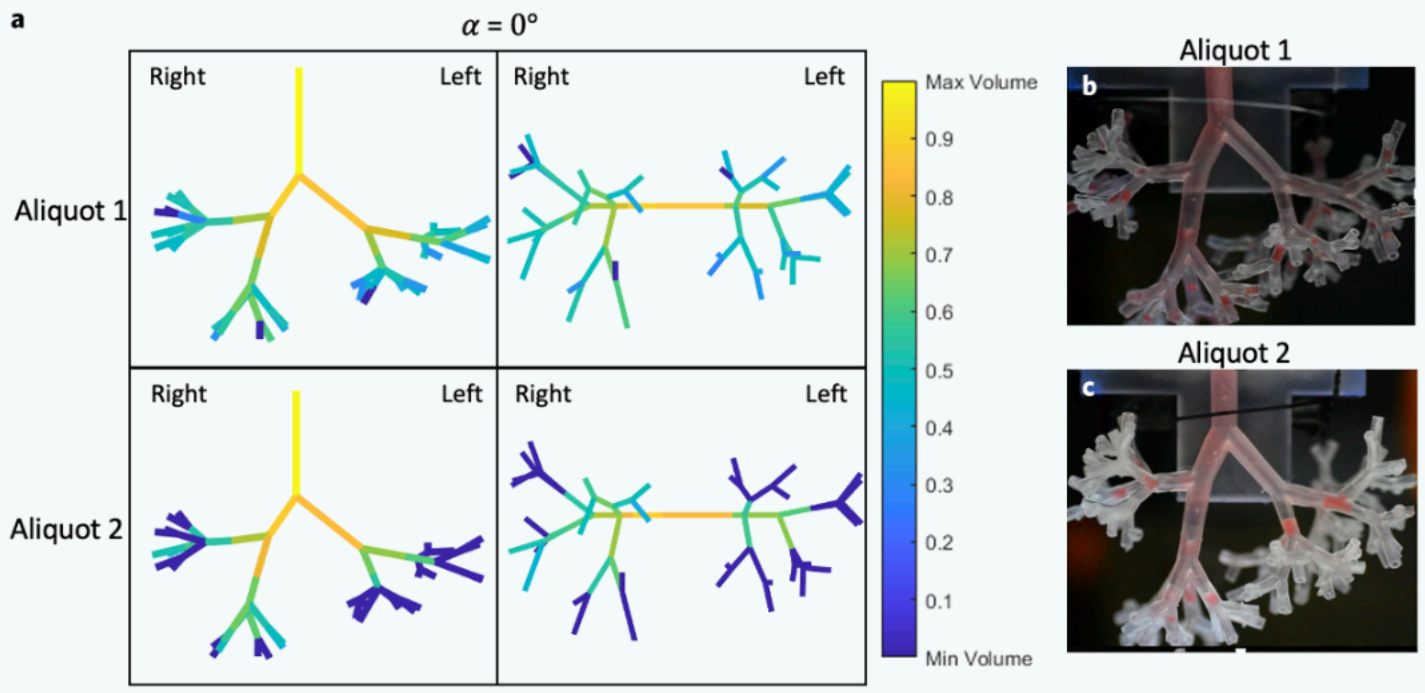


**Figure 4** (**a**) Heat maps representing surfactant distribution starting at the trachea (z = 0) to the fifth generation (z = 5). Two different views are shown at each orientation for aliquot 1 and aliquot 2 at $\alpha = 0°$. (**b**) Surfactant solution after propagation through the lung model for aliquot 1 and aliquot 2.

By adjusting the roll angle to 90° for the first aliquot, we observed significant increased gravitational effects to the right side of the lung with $DI_{UR} = 0.14 \pm 0.004$, $DI_{LR_a} = 0.13 \pm 0.012$, and $DI_{LR_p} = 0.13 \pm 0.008$ ($p < 0.05$). The sum of the indices indicated that the three lobes on the right side of the lung received majority of the surfactant compared to the left lobes with $DI_{LL} = 0.03 \pm 0.001$ and $DI_{UL} = 0.04 \pm 0.013$ ($p < 0.05$; **Fig. 3a, d** and Movie S3). The second aliquot at an orientation of $\alpha = -90^{o}$ primarily distributed to the left lobes, giving $DI_{LL} = 0.03 \pm 0.006$ and $DI_{UL} = 0.26 \pm 0.014$, and minimal surfactant reached the right lobes with $DI_{UR} = 0.07 \pm 0.015$, $DI_{LR_a} = 0.03 \pm 0.004$, and $DI_{LR_p} = 0.02 \pm 0.008$ ($p < 0.05$; **Fig. 3a, e** and Movie S4). Overall, we found that the most homogeneous delivery to the five lobes occurred when the lung model was in the supine position ($\alpha = 0^{o}$). When the model was rolled laterally to $\alpha = 90^{o}$ and $\alpha = -90^{o}$, the surfactant delivery occurred almost exclusively to the right lobe or the left lobe due to the gravity effect.

### Surfactant distribution to distal airways at $\alpha = 0°$, $\alpha = 90°$ and $\alpha = -90°$

We quantified the volume of surfactant plugs inside the $z = 0$ to $z = 5$ airways, i.e., a total of 63 airways, and constructed a series of heat maps to display the distribution of liquid surfactant in the airways. We found that

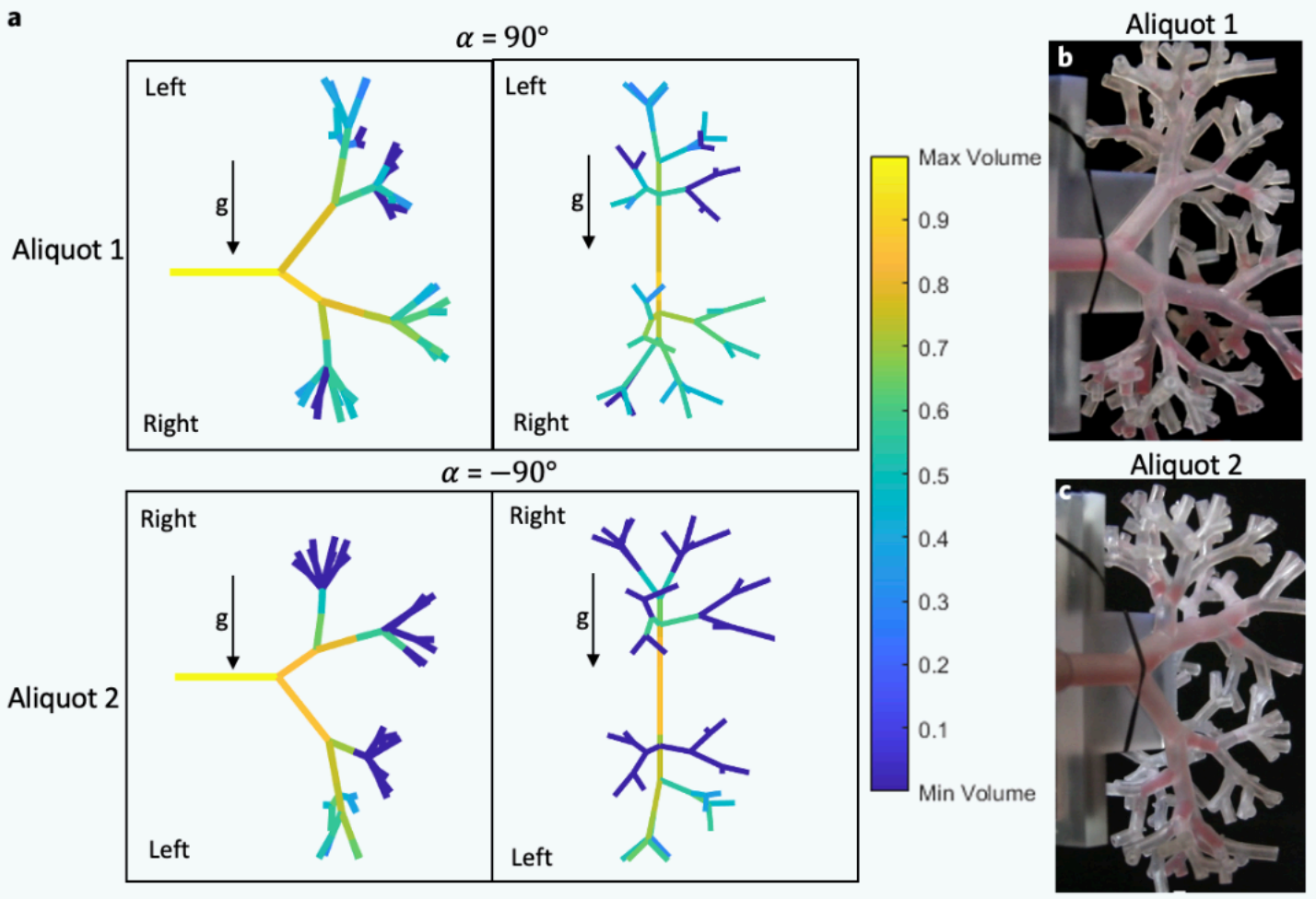


**Figure 5** (**a**) Heat maps representing surfactant distribution starting at the trachea (z = 0) to the fifth generation (z = 5). Two different views are shown at each orientation for aliquot 1 and aliquot 2 at $\alpha = 90^{\circ}$ and $-90^{\circ}$. The arrow indicates the portion of the lung that was gravitationally favored in each orientation, (**b**) surfactant solution after propagation through the lung model for aliquot 1, and (**c**) aliquot 2.

for the first aliquot at a supine position ($\alpha = 0^{\circ}$), the surfactant solution distributed relatively evenly among most of the airways. The posterior airways received slightly greater amounts of surfactant because they were gravitationally favored at this orientation (**Fig. 4a, b**). The right and left regions of the lung that divide at $z = 2$ received 57.5% ± 1.9% and 42.5% ± 1.9% of the instilled surfactant, respectively. The airways located in the fifth generation that appear in dark blue did not receive any surfactant due to the plug stalling in their prior generation. For the second aliquot delivered at $\alpha = 0^{\circ}$, airways in the right and left lungs received 52.7% ± 1.5% and 47.3% ± 1.5%. That is, the surfactant plugs divided relatively uniformly between the right and left lungs, with the posterior airways receiving a slightly greater volume of surfactant (**Fig. 4a, c**). We also found that a greater number of surfactant plugs stalled prior to reaching the fifth-generation airways for the second aliquot compared to the first aliquot.

To evaluate effects of orientation on the surfactant distribution to $z = 5$ airways, we positioned the model with the right lobes gravitationally favored at $\alpha = 90^{\circ}$ (**Fig. 5**). We quantified the volume of surfactant inside each airway for the first aliquot and found that 84.4% ± 2.2% of the surfactant solution entered the right lobes of the airway tree. This volume divided among the three right lobes relatively evenly, i.e., 34.7% ± 1.0% for UR, 33.3% ± 1.9% for $LR_p$, and 32.0% ± 2.9% for $LR_a$. The left region of the lung received a very small volume of surfactant with 15.6% ± 2.1% of the instilled dose. The volume of surfactant that entered the left lung also divided relatively evenly with 48.2% ± 2.8% for UL and 51.8% ± 2.6% for LL. Like in the supine position, plug stalling occurred inside the fourth-generation airways of the right lung, shown with the dark blue color in the heat map (**Fig. 5a, b**). The left lung that was not gravitationally favored received little surfactant because the small surfactant solution plugs propagating in these airways ruptured prior to reaching the fifth-generation airways. The plug rupture occurred due to depositing mass onto airways walls. We delivered the second aliquot with the left lung gravitationally favored at $\alpha = -90^{\circ}$ and found similar results to the first aliquot with the gravitationally favored lobes receiving a greater volume of surfactant (**Fig. 5a, c**). In this orientation, plug stalling was more prominent, causing a significant number of surfactant plugs to stop moving inside the third and fourth generations of airways.

## DISCUSSION

We designed and fabricated an asymmetric, eight-generation, lung airway tree model containing five lobes to study instilled liquid surfactant distribution due to air pressure. The UR, LL, and UL lobes broke off from the remainder of the model at $z = 2$, while the $LR_a$ and $LR_p$ lobes divided off the model at $z = 3$. Rolling the model from a supine position to $\alpha = 90^{\circ}$ increased the DI for the gravitationally favored lobes. This result is consistent with previous studies that used a symmetric model and showed that gravitationally favored lobes receive a larger volume of the instilled surfactant[19,31]. However, we also found that changes in distribution indices were smaller for the asymmetric model compared to the symmetric model. For example, in the asymmetric model with the first aliquot delivery, rolling the model from $\alpha = 0^{\circ}$ to $\alpha = 90^{\circ}$ increased the DI by 1.15-fold in the UR, 1.55-fold in the $LR_a$, and 1.50-fold in the $LR_p$, and decreased by 2.70-fold in the LL and 3.10-fold in the UL lobes. This change in the

orientation in the symmetric model from our previous study increased the DI by 3.25-fold in the UR and decreased by 16.7-fold in the UL lobes[31]. This indicates that the geometry of the airways plays a major role in determining surfactant distribution among different lobes. The delivery of the second aliquot after changing the orientation from $\alpha = 0°$ to $\alpha = -90°$ followed a similar pattern.

Further evaluation of surfactant distribution down to $z = 5$ showed similar gravitational effects, particularly at $\alpha = 90°$ and $-90°$, to those from our previous study with a symmetric lung model[31]. However, a key difference was significant plug stalling in the asymmetric model. Although plug stalling also occurred in the symmetric model, albeit to a much less extent, we overcame the limitation by completing plug volume estimations using single airway tubes of the respective airways in the model where plug stalling occurred. For example, if a surfactant plug stalled inside $z = 3$ airway, we used a single airway tube with the appropriate dimensions to that from the eight-generation model to propagate the plug and measure the volume loss over a given distance in order to estimate the remaining plug volume[31]. Using the volume loss estimations, we quantified the percentage of the instilled dose that was delivered to $z = 5$ airways[31]. For our asymmetric model, volume loss estimations were not feasible because of unique dimensions of each airway even within the same generation, preventing us from estimating plug volume inside $z = 5$ airways. We also found that the larger diameter airways in the $LR_a$ lobe caused significant surfactant deposition and led to plug rupture and free airflow through these airways due to path of least resistance and subsequent stalling of plugs in other lobes due to insufficient airflow through them[19,23,37]. This challenge limited our quantification of surfactant distribution downstream to generation $z = 5$.

Our computational and physical models of asymmetric lung airway tree feature physiologic geometries for airways including their unique bifurcation angles, lengths, and diameters and provide a new tool for both computational and benchtop studies[19,31,38]. Nevertheless, they still require design improvements to overcome existing limitations. For example, a potential approach to tackle the issue of plug stalling is to enclose the ends of terminal airways using compliant materials to mimic acini in order to prevent free airflow through airways without liquid plugs in them. In addition, adding the cyclic breathing capability will increase the physiological relevance to the clinical delivery of liquid surfactant during SRT. Overall, this research study provides a foundation to improve upon current studies and increase the success of liquid surfactant delivery in preterm neonates.

## CONCLUSIONS

We designed and fabricated a 3D, asymmetric lung airway tree model representing the conducting zone of a preterm neonate's lung. We used this model to study the distribution of a clinical surfactant under different orientations through imaging and quantification of propagating surfactant plugs in airways. Gravity had a similar effect on surfactant distribution in this asymmetric model compared to our previous symmetric model. However, the asymmetry of the individual airways, particularly differences in the diameter of airways of the same generation from left and right lungs, had significant effects on surfactant loss from propagating plugs onto airway walls, causing surfactant plugs to rupture prematurely and stalling of plugs elsewhere in the model. Further design improvements will be needed to facilitate liquid surfactant transport as it occurs in native lung airways during NSRT.

## ACKNOWLEDGMENTS

Financial support was provided by the National Science Foundation (grant no. 1904210).

## AUTHOR CONTRIBUTIONS

Hannah Combs: conceptualization (supporting); formal analysis (lead); validation (lead); methodology (lead); writing—original draft (lead); writing—review and editing (equal). Joseph Gaviloff: formal analysis (supporting). Lillian Beaty: formal analysis (supporting); methodology (supporting). Jacob Heiss: software (lead). Hossein Tavana: conceptualization (lead); funding acquisition; supervision (lead); writing—original draft (supporting); writing—review and editing (equal).

## DISCLOSURES

The authors have no conflicts to disclose. Ethics approval not required.

## DATA AVAILABILITY STATEMENT

The data that support the findings of this study are available from the corresponding author upon reasonable request.

## ORCID

Hannah Combs https://orcid.org/0009-0004-8833-8969
Jacob Heiss https://orcid.org/0009-0003-8987-976X
Lillian Beaty https://orcid.org/0009-0000-4422-8697
Joseph Gavriloff https://orcid.org/0009-0008-9721-3171
Hossein Tavana https://orcid.org/0000-0003-3872-1869

## REFERENCES

1. Zheng, Y., Fujioka, H., Grotberg, J.C. & Grotberg, J.B. Effects of inertia and gravity on liquid plug splitting at a bifurcation. *J. Bio. Eng.* **128**, 707–716 (2006).
2. Tu, J., Inthavong, K. & Ahmadi, G. Computational fluid and particle dynamics in the human respiratory system (pp. 19–44). (Springer, 2013).
3. West, J.B. *Respiratory physiology: The essentials*, (Wolters Kluwer Health/Lippincott Williams & Wilkins, Philadelphia, 2008).
4. Andreeva, A.V., Kutuzov, M.A. & Voyno-Yasenetskaya, T.A. Regulation of surfactant secretion in alveolar type II cells. *Am. J. Physiol. Lung. Cell. Mol. Physiol.* **293**, L259–L271 (2007).
5. Veldhuizen, E.J.A. & Haagsman, H.P. Role of pulmonary surfactant components in surface film formation and dynamics. *Biochim. Biophys. Acta, Biomembr.* **1467**, 255–270 (2000).
6. Gaver, D.P., Samsel, R.W. & Solway, J. Effects of surface tension and viscosity on airway reopening. *J. Appl. Physiol.* **69**(1), 74–85 (1990).
7. Grotberg, J.B. Respiratory fluid mechanics and transport processes. *Ann. Rev. Biomed. Eng.* **3**, 421–457 (2001).
8. Saad, S.M., Policova, Z., Acosta, E.J. & Neumann, A.W. Effect of surfactant concentration, compression ratio and compression rate on the surface activity and dynamic properties of a lung surfactant. *Biochim. Biophys. Acta.* **1818**, 103–116 (2012).
9. Tavana, H., Huh, D., Grotberg, J.B. & Takayama, S. Microfluidics, lung surfactant, and respiratory disorders. *Lab. Med.* **40**, 203–209 (2009).
10. Hamvas, A. Surfactant protein B deficiency: Insights into inherited disorders of lung cell metabolism. *Cur. Prob. Pedi.* **27**, 325–345 (1997).
11. Hentschel, R., Bohlin, K., van Kaam, A., Fuchs, H. & Danhaive, O. Surfactant replacement therapy: From biological basis to current clinical practice. *Pedi. Res.* **88**, 176–183 (2020).
12. Singh, P. *et al*. Diagnostic utility of lung ultrasound in predicting the need for surfactant therapy in preterm neonates with respiratory distress. *Front Pediatr.* **11**, 1307761 (2023).
13. Dyer, J. Neonatal respiratory distress syndrome: Tackling a worldwide problem. *P. T.* **44**, 12–14 (2019).
14. Polin, R.A. *et al*. Surfactant replacement therapy for preterm and term neonates with respiratory distress. *Pediatr.* **133**, 156–163 (2014).
15. Stevens, T.P. & Sinkin, R.A. Surfactant replacement therapy. *Chest*. **131**, 1577–1582 (2007).
16. Canadian Paediatric Society. Recommendations for neonatal surfactant therapy. *Paediatr. Child. Health.* **10**, 109–116 (2005).
17. Robertson, B. & Halliday, H.L. Principles of surfactant replacement. *Biochim. Biophys. Acta—Mol. Basis Dis.* **1408**, 346–361 (1998).
18. Zola, E.M. *et al*. Comparison of three dosing procedures for administration of bovine surfactant to neonates with respiratory distress syndrome. *J. Pedi.* **122**, 453–459 (1993).
19. Filoche, M., Tai, C.F. & Grotberg, J.B. Three-dimensional model of surfactant replacement therapy. *Proc. Natl. Acad. Sci. U S A.* **112**, 9287–9292 (2015).

20. Soll, R.F. & Morley, C.J. Prophylactic versus selective use of surfactant in preventing morbidity and mortality in preterm infants. *Cochrane Database Syst Rev*. **2**, CD000510 (2001).
21. Fernández, L.R. *et al*. Usefulness of lung ultrasound in the diagnosis and follow-up of respiratory diseases in neonates. *Anal. de Pedi. (English Edition)*. **96**, 252.e251–252.e213 (2022).
22. Liu, X., Si, S., Guo, Y. & Wu, H. Limitations of bedside lung ultrasound in neonatal lung diseases. *Front Pediatr.* **10**, 855958 (2022).
23. Fujioka, H., Takayama, S. & Grotberg, J.B. Unsteady propagation of a liquid plug in a liquid-lined straight tube. *Phys. Fluids (1994)*. **20**, 62104 (2008).
24. Kazemi, A. *et al*. Surfactant delivery in rat lungs: Comparing 3D geometrical simulation model with experimental instillation. *PLOS Comp. Biol.* **15**, e1007408 (2019).
25. Zheng, Y., Anderson, J.C., Suresh, V. & Grotberg, J.B. Effect of gravity on liquid plug transport through an airway bifurcation model. *J. Biomech. Eng.* **127**, 798–806 (2005).
26. Tavana, H. *et al*. Dynamics of liquid plugs of buffer and surfactant solutions in a micro-engineered pulmonary airway model. *Langmuir*. **26**, 3744–3752 (2010).
27. Copploe, A., Vatani, M., Amini, R., Choi, J.W. & Tavana, H. Engineered airway models to study liquid plug splitting at bifurcations: Effects of orientation and airway size. *J. Biomech. Eng. Trans. Asme.* **140**, 091012 (2018).
28. Elias-Kirma, S. *et al*. Towards homogenization of liquid plug distribution in reconstructed 3D upper airways of the preterm infant. *J. Biomech.* **122**, 110458 (2021).
29. Copploe, A., Vatani, M., Choi, J.W. & Tavana, H. A three-dimensional model of human lung airway tree to study therapeutics delivery in the lungs. *Ann. Biomed. Eng.* **47**, 1435–1445 (2019).
30. Cassidy, K.J. *et al*. A rat lung model of instilled liquid transport in the pulmonary airways. *J. Appl. Physiol. (1985)*. **90**, 1955–1967 (2001).
31. Combs, H., Shark, T., Heiss, J., Raessi, M. & Tavana, H. A quantitative study of transport of surfactant boli in a three-dimensional lung model of neonates. *J. Biomech. Eng.* **145**(2), 021006 (2022).
32. Phalen, R.F., Yeh, H.-C., Raabe, O.G. & Velasquez, D.J. Casting the lungs in-situ. *Anat. Rec.* **177**, 255–263 (1973).
33. Raabe, O.G. *Tracheobronchial geometry: Human, dog, rat, hamster: A compilation of selected data from the project respiratory tract deposition models* (U.S. Energy Research and Development Administration, Division of Biomedical and Environmental Research, Washington, DC, 1976).
34. Florens, M., Sapoval, B. & Filoche, M. An anatomical and functional model of the human tracheobronchial tree. *J. Appl. Physiol.* **110**, 756–763 (2010).
35. Majumdar, A. *et al*. Relating airway diameter distributions to regular branching asymmetry in the lung. *Phy. Rev. Lett.* **95**, 168101 (2005).
36. Weng, Z., Zhou, Y., Lin, W., Senthil, T. & Wu, L. Structure-property relationship of nano enhanced stereolithography resin for desktop SLA 3D printer. *Compos.—A: Appl. Sci. Manuf.* **88**, 234–242 (2016).
37. Halpern, D., Fujioka, H., Takayama, S. & Grotberg, J.B. Liquid and surfactant delivery into pulmonary airways. *Respir. Physiol. Neurobiol*. **163**, 222–231 (2008).
38. Weibel, E.R. & Gomez, D.M. Architecture of the human lung. *Science*. **137**, 577–585 (1962).


## SUPPLEMENTARY MATERIAL SECTION

The Supplementary Information are available at:
https://www.worldscientific.com/doi/suppl/10.1142/S2737599424500063.

**Movie S1.** Front view of propagation of first surfactant aliquot through airway tree at $\alpha = 0°$.

**Movie S2.** Front view of propagation of second surfactant aliquot through airway tree at $\alpha = 0°$.

**Movie S3.** Front view of propagation of first surfactant aliquot through airway tree at $\alpha = 90°$.

**Movie S4.** Front view of propagation of second surfactant aliquot through airway tree at $\alpha = -90°$.